ARTICLES
https://doi.org/10.1038/s41588-019-0462-3
nature genetics

Highly rearranged chromosomes reveal uncoupling between genome topology and gene expression

Yad Ghavi-Helm[1,2,3*], Aleksander Jankowski[1,3], Sascha Meiers[1,3], Rebecca R. Viales[1], Jan O. Korbel[1*] and Eileen E. M. Furlong[1*]

Chromatin topology is intricately linked to gene expression, yet its functional requirement remains unclear. Here, we comprehensively assessed the interplay between genome topology and gene expression using highly rearranged chromosomes (balancers) spanning ~75% of the *Drosophila* genome. Using transheterozyte (balancer/wild-type) embryos, we measured allele-specific changes in topology and gene expression in *cis*, while minimizing *trans* effects. Through genome sequencing, we resolved eight large nested inversions, smaller inversions, duplications and thousands of deletions. These extensive rearrangements caused many changes to chromatin topology, disrupting long-range loops, topologically associating domains (TADs) and promoter interactions, yet these are not predictive of changes in expression. Gene expression is generally not altered around inversion breakpoints, indicating that mis-appropriate enhancer–promoter activation is a rare event. Similarly, shuffling or fusing TADs, changing intra-TAD connections and disrupting long-range inter-TAD loops does not alter expression for the majority of genes. Our results suggest that properties other than chromatin topology ensure productive enhancer–promoter interactions.

Complex patterns of gene expression are controlled by enhancer elements, which can be located close to or far from (in genomic distance) their target genes[1–3]. How regulatory information is conveyed across such distances is a long-standing, poorly understood question[4]. In recent years, chromatin topology (that is, the three-dimensional conformation of DNA into complex topologies) has been suggested to play a key role in bringing enhancers into spatial proximity with their target genes[5]. The genome is organized into topologically associating domains (TADs), which represent contiguous genomic segments with a higher frequency of interactions within them than between them[6–9]. TADs are thought to create regulatory environments that facilitate enhancer function, and insulate promoters from ectopic activation by enhancers in a neighboring TAD. Evidence for this comes from the disruption of individual TAD boundaries in *cis*[7,10–14]. For example, a genomic inversion overlapping the boundary of the *Epha4* containing TAD leads to limb defects due to new interactions between *Epha4* enhancers and the *Wnt6* gene[10]. Such enhancer adoption[15] or hijacking[16] due to structural rearrangements affecting TADs has also been observed in cancer[16–20]. For example, in medulloblastoma, structural rearrangements facilitate new enhancer–promoter interactions and activation of the proto-oncogenes *GFI1* and *GFI1B*[16].

While these individual examples indicate that changing genome topology can have strong effects on gene expression, other studies suggest a more moderated role. For example, fusing or scrambling chromosomes in yeast has little effect on gene expression[21,22], perhaps due to the predominantly promoter-proximal regulation in yeast. In *Drosophila*, where enhancers are comparatively more distal, deletions[23] or engineered inversions within three testis-specific gene clusters[24] had little impact on gene expression, although their impact on chromatin topology was not assessed. Similarly, a series of increasingly large deletions overlapping a TAD boundary in the mouse *HoxD* locus had little effect on limb bud expression[25]. It was only with larger deletions (>40 kilobases (kb)) that expression changes and ectopic interactions across the TAD boundary were observed[25]. Perhaps even more striking, depletion of CTCF[26,27] and cohesin[28–30] proteins in *trans* led to a very dramatic reduction in TAD insulation for the majority of TADs, yet this had only moderate effects on gene expression[26,28,29]. This may reflect the inherent difference between weakening TAD boundaries due to protein depletion in *trans*[27,29,31], compared with completely altering TAD structure due to rearrangements in *cis*[10–12]. These results indicate that much more extensive genetic manipulations are needed to resolve the functional role of genome topology in enhancer–promoter communication.

To more systematically assess the functional relationship between chromatin topology and gene expression, we took advantage of the highly rearranged nature of balancer chromosomes in *Drosophila melanogaster*. We sequenced the genome of a 'balancer' line, whose second and third chromosomes contain eight large nested inversions, several smaller inversions, duplications and thousands of deletions. The functional impact of these genetic perturbations on genome topology and gene expression was assessed in *cis* in heterozygote embryos, using allele-specific Hi-C and RNA sequencing (RNA-Seq). Despite major changes in genome organization, only a few hundred genes have moderate changes in expression, indicating that only a subset of genes are sensitive to changes in their topology. Rearrangements that alter TAD boundaries or reshuffle TADs, for example, impact the expression of only a subset of the associated genes, suggesting that enhancer hijacking is a rare event. Genetic variants that resize TADs, cause intra-TAD changes in promoter interactions or break long-range inter-TAD loops are generally not correlated with changes in gene expression. Although gene expression

[1]European Molecular Biology Laboratory, Genome Biology Unit, Heidelberg, Germany. [2]Present address: Institut de Génomique Fonctionnelle de Lyon, Univ Lyon, CNRS UMR 5242, Ecole Normale Supérieure de Lyon, Université Claude Bernard Lyon 1, Lyon, France. [3]These authors contributed equally: Yad Ghavi-Helm, Aleksander Jankowski, Sascha Meiers. *e-mail: yad.ghavi-helm@ens-lyon.fr; korbel@embl.de; furlong@embl.de

at distinct loci is influenced by topology, our more global data suggest that this is not generalizable; the expression of many genes appears resistant to rearrangements within their regulatory domain.

Results

***Drosophila* balancer chromosomes as a source of highly rearranged chromosomes.** Balancers are highly rearranged chromosomes that carry multiple nested inversions, suppressing the recovery of genetic recombinants between homologous chromosomes during meiosis. They were generated roughly 60 years ago[31,32] by combining a recessive lethal mutation with inversions, which were then extended further by X-ray irradiation to increase the balancer's capacity to suppress recombination across large stretches of the chromosome[33]. Balancers are therefore typically homozygous lethal and maintained in *trans* to a non-balancer homologous chromosome. Here, we used a 'double-balancer' line carrying rearranged chromosomes for both the second (CyO)[31] and third (TM3)[32] chromosomes, together covering 76% of the *Drosophila* genome (Fig. 1a). We crossed the double balancer to an isogenic wild-type line (Supplementary Fig. 1a and Methods). *Trans*-heterozygous adults from the F_1 generation were backcrossed to the wild-type parental line, and this pool of N_1 embryos was used for all embryonic experiments (Supplementary Fig. 1a,b and Methods). Importantly, this ensures that the N_1 generation is devoid of homozygous balancer embryos, which are embryonic lethal and therefore likely to exhibit indirect effects on gene expression. Allele-specific chromosome conformation capture (Hi-C and Capture-C) and RNA-Seq were used to measure changes in chromatin organization and gene expression from both chromosomes. This design thereby facilitates a direct comparison between genome topology and gene expression in *cis*, while minimizing *trans* effects.

To identify single nucleotide variants (SNVs) and structural variants (Methods), the DNA of F_1 and wild-type adults was sequenced using mate-pair[34] and whole-genome sequencing (WGS). We detected 761,348 SNVs on chromosome 2 and 3 compared with the reference genome, of which 38.9% are balancer specific and 29.5% are wild-type specific (Fig. 1b). An allele-specific SNV occurs on average every 210 bp, allowing sequencing reads to be efficiently assigned to the balancer or wild-type haplotypes. We integrated three approaches (paired-end, split read and read depth[35]) to identify structural variants with high confidence (Methods), obtaining 6,180 small (15–49 bp), 687 medium (50–159 bp) and 434 large (0.16–5.2 kb) deletions, in addition to 122 tandem duplications (from 400 bp to 33 kb) (Fig. 1c–e). This is in line with previous *Drosophila* population studies, which identified polymorphic duplications to be on average larger but less numerous than deletions[36,37]. The accuracy of structural variant predictions was confirmed by PCR on randomly selected loci for medium and large deletions (validation rates: 24/25 (medium size); 49/50 (large); Supplementary Table 1).

The two balancer chromosomes contain eight large nested inversions (Fig. 1c), whose approximate cytological locations were characterized by karyotyping[38]. Using mate-pair sequencing, we mapped their breakpoints to base-pair resolution in 14 out of 16 cases (Fig. 1c and Supplementary Table 2). Most of the newly formed junctions resulted in a deletion (in one case, ~17.5 kb) followed by a small duplication (four cases; up to 281 bp), as observed in humans[39]. Only one inversion had a precise re-ligation. We confirmed all breakpoints using two independent approaches. First, recent independent sequencing of the second[40] and third[41] balancer chromosomes precisely matched our breakpoints in 12 cases. Second, we performed allele-specific Hi-C on the pool of N_1 embryos collected at 4–8 h after egg laying (stages 8–11) (Methods and Supplementary Table 3). After separating the reads from each haplotype, Hi-C contact maps were generated for both the balancer and wild-type chromosomes. The inversions are visible as strong signals off the diagonal, with a characteristic 'bowtie' shape when mapped to the reference genome (Fig. 1f). The location of the breakpoints perfectly recapitulates the expected karyotype information. In addition to these large inversions, we identified a 38-kb inversion and three non-tandem duplications on the balancer chromosomes, including a 258-kb inverted duplication (Supplementary Fig. 2a,b).

Genomic perturbations accumulate in balancer chromosomes. As the double balancer is only viable in a heterozygous state, there is little selective pressure to eliminate deleterious mutations. Balancer chromosomes also suppress recombination in the broad vicinity of the inversion breakpoints, as recently confirmed[40,41]. The combination of these two properties means that balancers act as mutational sinks, accumulating deleterious structural variants and SNVs over time. This is exactly what we observe for the double-balancer line: the balancer chromosomes have ~1.3 times more allele-specific SNVs compared with wild-type chromosomes (Fig. 1d). Many balancer-specific SNVs are not found in a well-studied wild population (the *Drosophila* Genetic Reference Panel (DGRP))[36,42], with a lower fraction (86.1%) of balancer-specific SNVs present in DGRP lines compared with the wild-type strain (92.1%). Balancer chromosomes also contain more deletions (especially larger ones) compared with their wild-type homologs (a ratio of 1.9 for deletions ≥160 bp; Fig. 1d). Balancer chromosomes have therefore accumulated many genetic variants not present in homozygous viable lines.

Many structural variants could affect functional elements. For example, deletions impact more DNase I hypersensitive sites (DHSs) at matching developmental stages[43] in the balancer chromosomes than the wild-type chromosomes (82:53) (Fig. 1d and Supplementary Fig. 2c). Similarly, structural variants impact more protein-coding genes on balancer chromosomes. The breakpoints of the large nested inversions, for example, disrupt genes in 12 out of 16 cases, including *Glut4EF* (a transcription factor involved in developmental patterning and morphogenesis) and *p53* (a tumor suppressor). A 17.5-kb deletion at the 20.32-megabase (Mb) breakpoint on chromosome 3R removes *CG42668* (a predicted sterol-binding protein) in the balancer line (Supplementary Fig. 2d,e), while a 258-kb inverted duplication increases the copy number of 31 genes and disrupts one gene (*CG31886*) that exists in two truncated copies (Supplementary Fig. 2a,b).

Balancer chromosomes therefore contain many structural variants affecting both regulatory and coding regions. These chromosomes thereby provide a rich resource of genomic rearrangements, including inversions, duplications and deletions, which can be used to systematically assess the functional impact of changes in chromatin organization on gene expression.

Genome rearrangements effect expression of a small proportion of genes. To assess the impact of the extensive changes in genomic structure on gene expression, we performed allele-specific RNA-Seq on N_1 embryos at 6–8 h after egg laying (stages 10 and 11; Supplementary Table 4). To control for possible effects of maternally deposited RNA, embryos were obtained from crosses performed in both directions (Supplementary Fig. 1a and Methods). Sequencing reads were separated based on haplotype-specific SNVs and tested for allele-specific expression (Methods). Of the 5,357 testable genes (on chromosomes 2 and 3) with sufficient allele-specific reads, 512 (9.6%) had significant (5% false discovery rate (FDR)) differential expression between the balancer and wild-type haplotypes, 343 (6.4%) of which had a >1.5-fold change (Fig. 2a). Differentially expressed genes have no specific enrichment for biological process or function (Methods).

We confirmed the near absence of *trans* effects (that is, the expression of genes on chromosome 3 does not depend on the presence of a chromosome 2 balancer) and vice versa (Methods). The differential expression of only 99 out of 5,981 genes (1.66%)

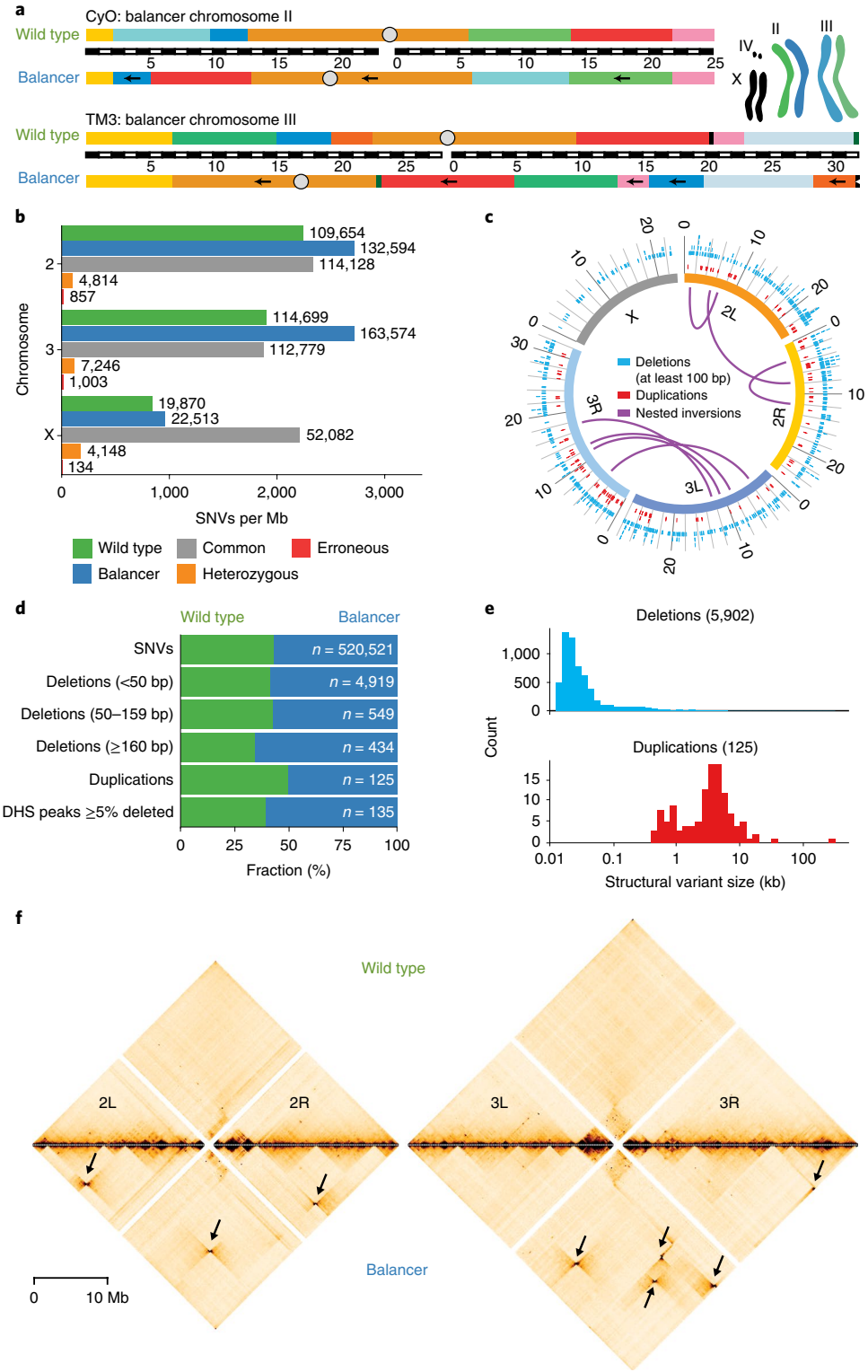

Fig. 1 | Genomic variation in balancer and wild-type chromosomes. a, The *D. melanogaster* balancer chromosomes CyO and TM3 carry multiple nested inversions. Arrows indicate segments on the balancer chromosomes that have an opposite orientation compared with the wild type. Black bars with white dashes indicate chromosome size (Mb). The schematic depicts the genotype of the heterozygous (F_1) fly line used. **b**, Number of SNVs specific to the wild type (green) and balancer (blue), or common to both haplotypes (gray), heterozygous (orange) or erroneous (red), per Mb for each chromosome. **c**, Circos plot representing the distributions of structural variants (deletions >100 bp, blue; duplications, red; and nested inversions, purple) in balancer and wild-type chromosomes. Variants common to both are omitted. **d**, Fraction of SNVs, deletions (<50 bp, 50–159 bp or ≥160 bp), duplications and DHSs (deleted by ≥5% of their length) specific to wild-type (green) or balancer (blue) haplotypes. **e**, Size distributions of allele-specific deletions (blue) and duplications (red). **f**, Allele-specific Hi-C contact maps for wild-type (top) and balancer chromosomes (bottom), relative to the reference assembly (dm6). Bowtie-shaped contacts (arrows) correspond to the nested inversions characteristic of balancer chromosomes.

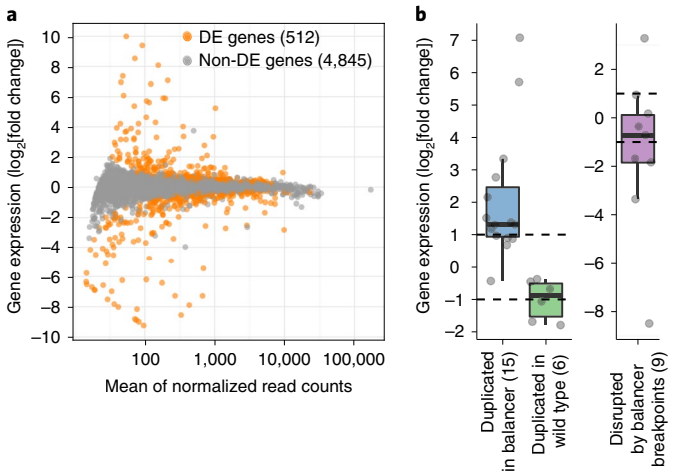

Fig. 2 | Impact of chromosomal rearrangements on gene expression. **a**, Chromosomal rearrangements generally have a modest effect on gene expression, as shown by a MA plot of genome-wide differential gene expression between wild-type and balancer haplotypes. Differentially expressed (DE) genes ($n=512$) are shown in orange (two-sided Wald test; 5% FDR). **b**, Change in gene expression ($\log_2$[fold change]) for testable genes fully duplicated ($n=21$) or disrupted by balancer breakpoints ($n=9$). Points represent individual genes; the center line is the median; box limits are the upper and lower quartiles; whiskers represent 1.5× the interquartile range; and dashed lines are the expectation for duplications (two-fold increase or decrease).

could be explained by *trans* effects (Supplementary Fig. 3a). While higher than expected from biological noise (0.45%; Supplementary Fig. 3b), this percentage is notably smaller than the total fraction of differentially expressed genes in the F_1 generation (6.1%).

Copy number variants (CNVs; for example, duplications or deletions) that fully contain a gene provide a clear prediction of the impact of structural rearrangements on gene expression, and serve as a positive control. Reassuringly, the majority of fully duplicated genes display the expected twofold change in allelic expression (Fig. 2b), showing the sensitivity of the data. For example, in the context of a 258-kb balancer-specific duplication, the majority of expressed genes have the expected twofold increase in allelic expression (Supplementary Fig. 2a). This trend is also observed for genes with a partial duplication or deletion, but to a lesser extent, as expected (Supplementary Fig. 3c). In total, 50 of the 512 differentially expressed genes (42/343 genes with a >1.5-fold change) are likely explained by CNVs. An additional 45 of the 343 differentially expressed genes with a >1.5-fold change have aberrant transcriptional starts, most likely caused by the insertion of a transposable element in their vicinity. This signal can cause haplotype-imbalanced read counts, which likely explains their differential expression.

In summary, the large diversity of structural variants between the balancer and wild-type chromosomes has moderate effects on gene expression with ~10% (512/5,357) of genes affected on the balancer chromosome. Of these, a relatively small proportion (~18%; 95/512) can be explained by genetic variation directly impacting the genes themselves. In the subsequent analysis, we examine whether changes in chromatin topology can explain the expression changes of the remaining ~80% of genes.

Chromosomal rearrangements that affect TAD size have little effect on gene expression. To assess the impact of genome rearrangements on chromatin topology, we used allele-specific Hi-C data and estimated the location of TAD boundaries in each haplotype using insulation scores[44]—a normalized measure of Hi-C contacts between a window upstream and downstream (Methods). Insulation score profiles are globally highly correlated between biological replicates for each haplotype (Supplementary Fig. 4a), and between the wild-type and balancer chromosomes (Fig. 3a), indicating that structural variants have a minor impact on chromatin structure genome wide. TAD boundaries were defined in both haplotypes as the local minima in insulation score profiles. On chromosomes 2 and 3, we identified 771 TADs in the wild-type haplotype and 761 TADs in the balancer haplotype, with a median size of 125 kb.

Comparing the location of TAD boundaries revealed that ~12% are lost (or shifted by >25 kb) in either haplotype (Methods): 96 out of 767 wild-type boundaries are lost in the balancer, while 86 are gained. Differentially expressed genes are moderately enriched within ±10 kb of perturbed TAD boundaries (Fig. 3b, Supplementary Fig. 4b and Methods): 12.2% (29/237) of testable genes within ±10 kb of a perturbed boundary are differentially expressed genes, compared with 8.5% (155/1,821) around non-perturbed boundaries ($P=0.047$, two-sided binomial test). The effect increases for genes with a >1.5-fold change: 9.7% (23/237) of differentially expressed genes compared with 4.9% (90/1,821) (Fig. 3c and Supplementary Fig. 4c; $P=0.0023$). There is therefore a significant enrichment of differentially expressed genes within 10 kb of a perturbed boundary; however, the actual fraction of affected genes is low (only ~10–12% of genes within 10 kb, and ~6% (29/512) of all differentially expressed genes).

Next, we assessed the effect of inversion breakpoints on TAD size by separating balancer breakpoints falling inside a TAD (disrupting it) from those located close to TAD boundaries. The resulting 16 breakpoints (14 from the large nested inversions and two from a 38-kb inversion) that are located away (>13 kb) from a TAD boundary result in resized (shuffled) TADs that typically still use the existing boundaries (Fig. 3d–g). In fact, the vast majority of TADs (88%) have unchanged boundaries despite drastic rearrangements of the genome. The location of TAD boundaries therefore seems to be mostly driven by the sequence of the boundary region itself, rather than the sequence or expression status within the TAD.

Although the position of the boundaries has not changed, the size of these shuffled TADs often changed dramatically (Fig. 3h). The breakpoints split the 16 disrupted TADs into 32 'halves', which are rearranged differently in the balancer. In five cases, the 'halves' are in a TAD over 50 kb bigger in the balancer, and in ten cases they are in a TAD over 50 kb smaller. Some 443 genes are located in the 16 resized TADs, of which 322 carry allele-specific SNVs (161 of these genes are expressed, while the remainder have little or no expression at these embryonic stages). Remarkably, these changes in TAD size are not correlated with changes in gene expression (Fig. 3i). A total of 23 genes (out of 161) are differentially expressed ($P=0.040$, two-sided Fisher's exact test), only 16 of which are to a >1.5-fold change ($P=0.067$, two-sided Fisher's exact test). Interestingly, none of the inactive genes within shuffled TADs was ectopically expressed, suggesting that expressed genes may be more sensitive to changes in their topology.

The expression of the majority of genes within shuffled TADs is not affected by changes in their regulatory environments. To explore this further, we examined the location of differentially expressed genes with respect to the breakpoints: differentially expressed genes within disrupted TADs are significantly closer (median distance: 35 kb) to inversion breakpoints compared with non-differentially expressed genes (Fig. 3j; $P=0.017$, two-sided Kolmogorov–Smirnov test). Therefore, changing the regulatory context within a TAD by inversions that essentially swap TAD parts leads to significant changes in the expression of some genes that tend to be close to the breakpoint, presumably due to altered enhancer–promoter interactions. However, it is important to note that only a fraction of genes (12/38 expressed genes and 0/34 lowly expressed/inactive

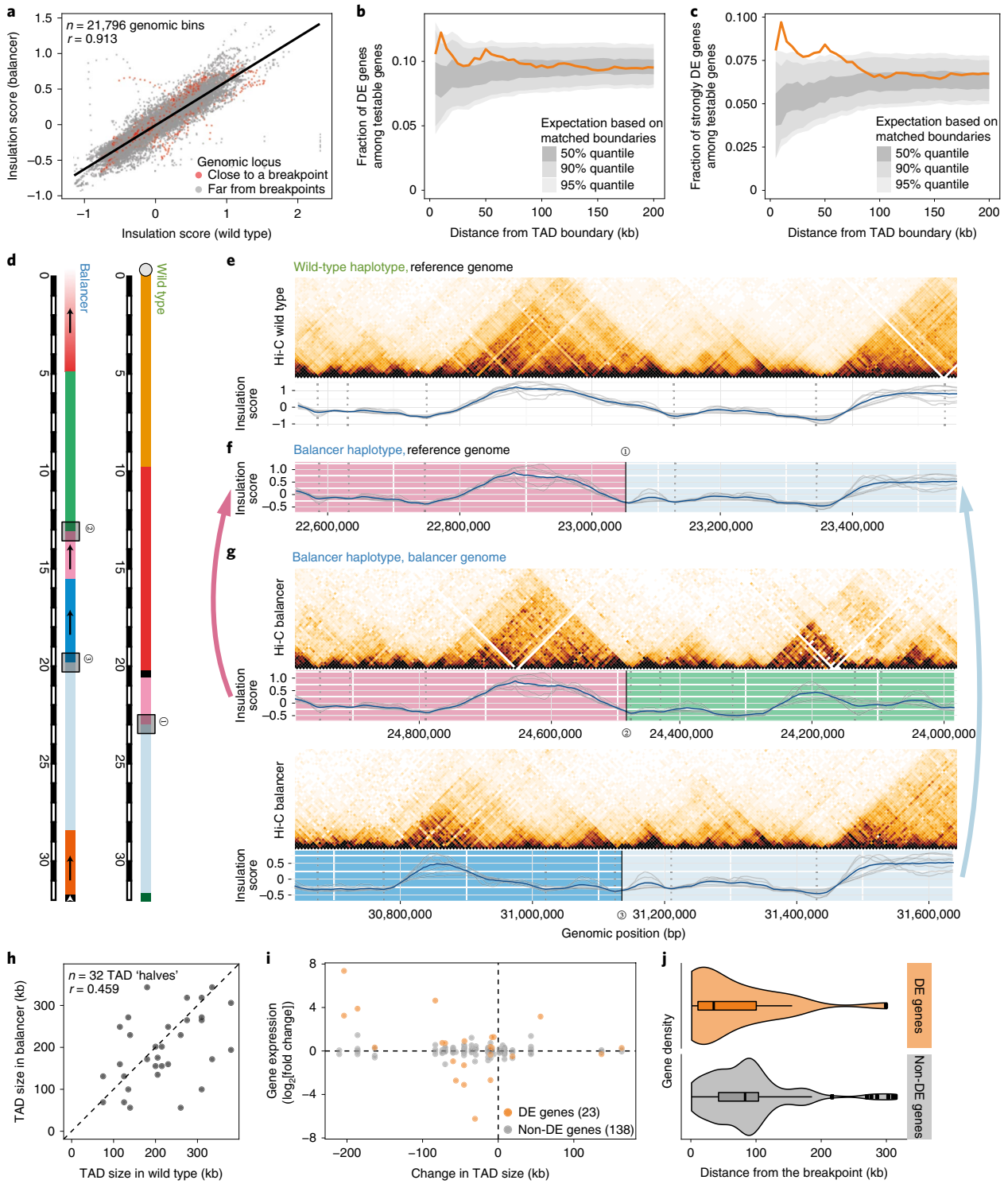

Fig. 3 | Extensive changes in TADs have limited impact on gene expression. a, Insulation scores (averaged across different window sizes) are highly correlated between wild-type and balancer haplotypes, even close to inversion breakpoints (red). The Pearson correlation coefficient (*r*) is indicated. **b**,**c**, Fraction of all DE genes (**b**) or those with a >1.5-fold change (**c**) at varying distances from 182 perturbed TAD boundaries (orange). The 50, 90 and 95% percentiles (gray ribbons) are shown from randomly sampled matched boundaries. **d**, Schematic of the breakpoint on chromosome 3R at 23.05 Mb in the wild-type (1) and genomic sequences on each side of the breakpoint in the balancer haplotype (2 and 3). **e**, Top, wild-type Hi-C contact map of a 1-Mb region around the breakpoint (1) from **d**. Bottom, wild-type insulation scores for seven window sizes (50–195 kb; gray lines), the average profile (blue) and TAD boundaries (gray dotted lines). **f**, Balancer insulation score profile for the region shown in **e** in wild-type assembly or **g**, balancer assembly, for breakpoints (2) and (3); *x* axis, genome coordinates (base pairs, dm6); *y*-axis, insulation score. **h**, Changes in TAD size due to inversions. Pearson correlation coefficients (*r*) are indicated. **i**, Changes in TAD size do not correlate with changes in gene expression ($\log_2$[fold change]) of DE genes or non-DE genes. **j**, DE genes (orange, 23 genes) in disrupted TADs are significantly closer to the inversion breakpoints than non-DE genes (gray, 138 genes). Center lines represent the median; box limits are the upper and lower quartiles; whiskers show 1.5× the interquartile range; and points are outliers ($P = 0.017$, two-sided Kolmogorov–Smirnov test).

genes) within 35 kb of a breakpoint change expression. In six of the 16 TADs, it is the gene closest to one side of the breakpoint that is differentially expressed (Supplementary Fig. 4d), suggesting mis-regulation due to new local positioning close to an enhancer. However, in the other ten cases, there are one or more unaffected genes closer to the breakpoint than a differentially expressed gene, indicating that proximity alone is not sufficient to activate all genes' expression. In addition, the absolute expression level of differentially expressed genes within disrupted TADs is not significantly different from non-differentially expressed genes (Supplementary Fig. 4e; $P=0.09$, two-sided Wilcoxon test). Therefore, although productive enhancer–promoter interactions can be formed de novo (for example, as seen in the 38-kb inversion (discussed below)), the majority of genes are not mis-regulated. This suggests selectivity in many enhancer–promoter interactions that cannot be explained by regulatory distance alone.

Changes in gene expression are correlated with local changes in genome topology. To explore the impact of changes in intra-TAD contacts (putative enhancer–promoter interactions) on gene expression, we performed Capture-C to generate high-resolution views of promoter topologies. Libraries were generated on the same pool of N_1 embryos as Hi-C, using probes designed to hybridize equally to the two haplotypes and capture promoters of 221 differentially expressed genes and 68 non-differentially expressed 'control' genes (Supplementary Tables 5 and 6 and Methods). Differential interactions were defined by comparing the interaction count of balancer versus wild-type haplotypes using both Hi-C and Capture-C data (Methods). Among 216,066 tested pairwise interactions between 5 kb Hi-C bins, 4,329 had significant differential contacts not explained by overlapping CNVs. Among the 59,605 tested interactions from the Capture-C viewpoints, 931 had differential contacts at the level of individual restriction fragments. Neighboring differential fragments within 1 kb were clustered to form 445 differentially contacted regions.

First, we focused on differentially expressed genes and plotted the differential contact density from their transcription start sites (TSSs) (Fig. 4a,b). Genes with differential expression generally have twice as many differential contacts from their promoters: differentially expressed genes have on average 0.48 differential Hi-C contacts within ±100 kb from their TSS, while non-differentially expressed genes have 0.20 ($P=0.006$, two-sided Kolmogorov–Smirnov test; Fig. 4a). Similarly, with Capture-C, differentially expressed genes have on average 3.59 differential contacts within ±100 kb from their TSS, while non-differentially expressed genes have 1.46 ($P=0.033$; Fig. 4b). This effect is more pronounced for genes with a >1.5-fold change in expression (Supplementary Fig. 5a,b). The effect vanishes at larger distances (>50 kb). Genes with changes in their expression therefore have a small, but significant, increase in local (≤50-kb) differential contacts with their promoters.

Interestingly, such differential interactions from the promoters of differentially expressed genes often involve the promoters of other differentially expressed genes—an observation that occurs more often than expected by chance (Supplementary Fig. 5c). For 14 out of 18 such pairs of differentially expressed genes linked by a differential contact, the direction of change is the same for both genes' expression (Supplementary Fig. 5d ($P=0.03$, two-sided binomial test) and Supplementary Table 7). The promoters of *Dscam4* and the long non-coding RNA *CR43953*, for example, are in proximity in the balancer, but not the wild-type (40-fold increased Hi-C contact), which is associated with a strong downregulation of both genes' expression in the balancer (Fig. 4c). Conversely, three differential contacts between the promoter of *subdued* (a chloride channel) and multiple promoters of *CG6231* (a predicted transmembrane transporter), located 10–20 kb away (Fig. 4d), are reduced on the balancer chromosome, which is associated with a roughly twofold decrease in both genes' expression. The concordance in the changes between both genes' expression and their promoter interactions suggests co-regulation of gene pairs, perhaps in a transcriptional hub type of conformation.

Changes in genome topology are not predictive of changes in gene expression. As shown above, genes with changes in their expression have a small but significant enrichment for differential promoter contacts. To test whether the converse is true (that is, whether changes in three-dimensional proximity (Hi-C contacts) are predictive of changes in gene expression), we extracted differential contacts that had a TSS at either of the two contacting loci. Of the 4,329 differential Hi-C contacts (after filtering for CNVs), 1,063 (24.6%) are associated with a promoter of a testable gene. Focusing on these promoters with differential contacts reveals no correlation between promoter contact frequency (Hi-C fold change) and gene expression (Fig. 4e). Only 25% (265/1,063) of differential contacts at promoters are associated with a change in gene expression. Similarly, with Capture-C, although the majority (76%) of tested promoters were differentially expressed genes, differential promoter contacts are not correlated with differential gene expression (Fig. 4f and Supplementary Fig. 5b,e), indicating that this observation is likely not due to limited resolution. Rather, there are many differential contacts at promoters that do not correlate with changes in gene expression.

Taken together, our results indicate that differential gene expression is globally correlated with local changes in genome topology (or contacts), as observed at individual loci: genes that change in expression generally have twice as many differential contacts at their promoters compared with non-differentially expressed genes. However, going in the other direction, changes in genome topology at promoters are not globally correlated with changes in gene expression: 75% (798/1,063) of all promoter contacts at testable genes (differential promoter contacts) can change with no measurable effect on gene expression. These results highlight an inherent robustness within regulatory landscapes, where many changes in genome topology—even at promoters—are buffered at the level of changes in gene expression.

Loss of long-range chromatin loops has little impact on gene expression. Long-range inter-TAD loops that span multiple TADs have been observed in many species, including *Drosophila*[9].

Fig. 4 | Changes in promoter contacts and their relationship to gene expression. a,**b**, Top, positional distribution of differential Hi-C (**a**) and Capture-C (**b**) contacts originating from TSSs of DE (orange) and non-DE (gray) genes. All genes' TSSs are centered at 0 with their direction of transcription to the right. 95% confidence bands (shaded ribbons) were estimated using bootstrapping. Bottom right, heat maps of differential contacts for 200 randomly sampled DE genes (Hi-C; **a**) and for all captured DE genes (Capture-C; **b**). Bottom left, expression of genes shown in each heat map. **c**,**d**, Downregulated genes (*CR43953* and *Dscam4* in **c**, and *CG6231* and *subdued* in **d**) have differential Hi-C contacts, with either increasing (red in **c**) or decreasing (blue in **d**) proximity in the balancer. From top to bottom, wild-type and balancer Hi-C contact maps; $\log_2$[fold change] before normalization (balancer/wild type; red/blue); DHSs; gene models; and differential gene expression (balancer/wild type). DE genes are shown in orange, non-DE genes are in blue and non-tested genes (lowly expressed or lacking SNVs) are in gray. Arrowheads highlight differential contacts and the affected genes. **e**,**f**, Hi-C (**e**) and Capture-C (**f**) differential contacts are plotted against changes in expression of all genes with a TSS in the two interacting genomic bins. DE genes are highlighted in orange.

They typically involve co-regulated active genes; for example, *sns* and *hbs* in *Drosophila*[9], or inactive Polycomb repressed genes[45]. Six such long-range chromatin loops span across the nested inversion breakpoints, allowing us to assess whether genome reorganization affects long-range looping and how this impacts gene expression. In two cases (*sns*/*hbs* and *Wbp2*/*Nufip*), the loop is still present (although

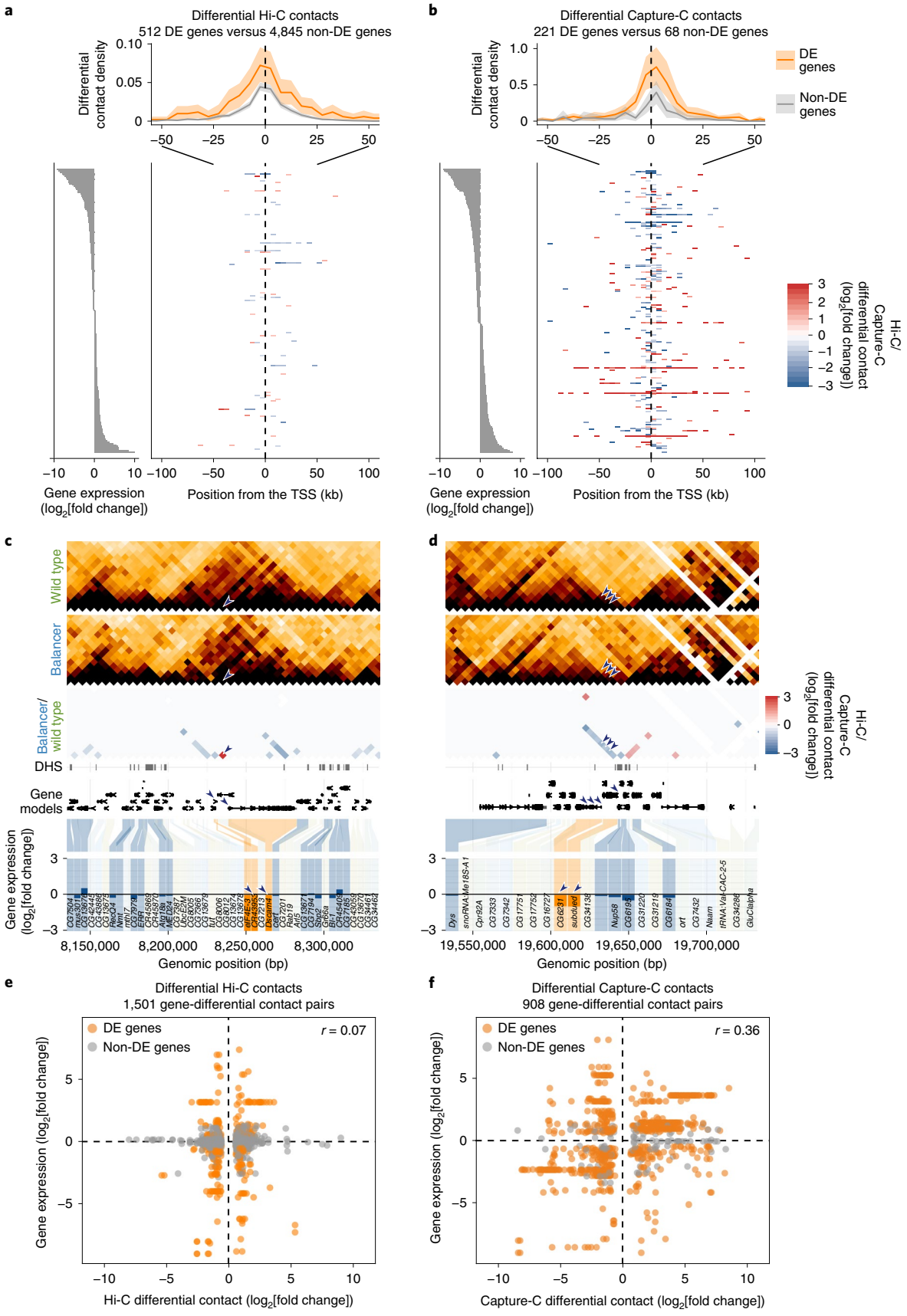

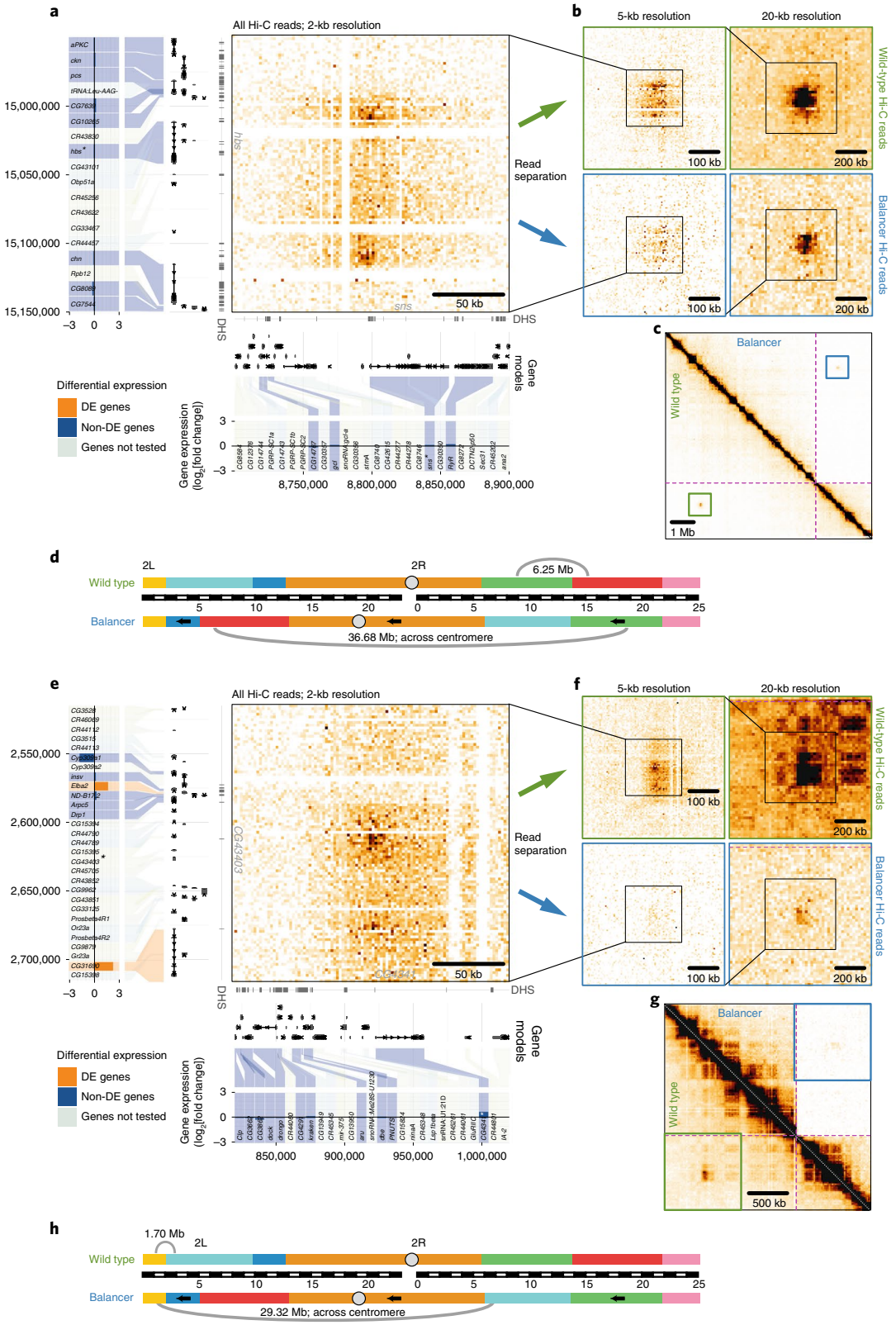

Fig. 5 | Loss of long-range chromatin loops has little impact on gene expression. a,**e**, Hi-C contact maps (2-kb resolution; all Hi-C reads) showing long-range loops between *hbs* (left) and *sns* (bottom) (**a**) and between *CG43403* (left) and *CG4341* (bottom) (**e**). Locations of DHSs, gene models and differential gene expression (balancer/wild-type) are shown. DE genes are in orange, non-DE genes are in blue and non-tested genes (lowly expressed or lacking SNVs) are in gray. **b**,**f**, Magnified wild-type (top) and balancer (bottom) Hi-C contact maps at 5-kb (left) and 20-kb resolution (right), showing a slight (**b**) or strong (**f**) decrease in the strength of long-range loops. **c**,**g**, Zoomed-out Hi-C contact maps showing the locations of the long-range loops between *sns* and *hbs* (**c**) and between *CG4341* and *CG43403* (**g**) in the wild-type (bottom left) and balancer (top right) haplotypes. Locations of inversion breakpoints are indicated by purple dotted lines. **d**,**h**, Schematics depicting the locations and distances of both loops on chromosome 2 in wild-type (top) and balancer (bottom) haplotypes with respect to the inversion breakpoints.

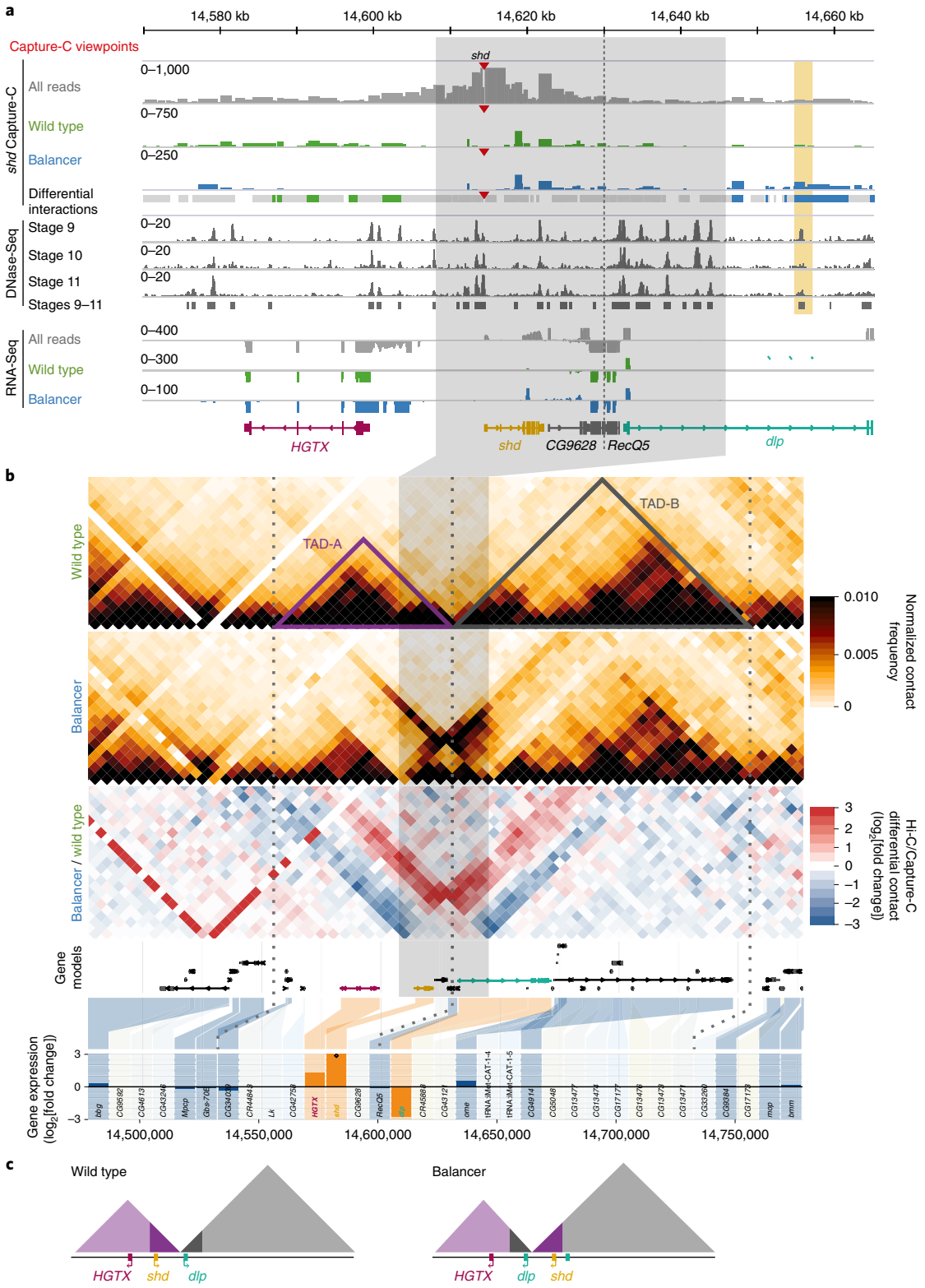

Fig. 6 | Chromatin organization and expression around a 38-kb inversion. a, Top, Capture-C tracks (all reads, gray; wild-type-specific reads, green; and balancer-specific reads, blue) for the *shd* viewpoint (red triangle) in the vicinity of a balancer-specific inversion in chromosome 3L (gray highlight). The dashed vertical line indicates the TAD boundary. Differential Capture-C contacts stronger in the wild-type (green), stronger in the balancer (blue) or not significantly changed (gray) are highlighted. Middle, DHS signal at stages 9–11. Bottom, RNA expression (all reads and allele specific). Gene models are shown underneath. A differential contact is formed between the *shd* promoter and a DHS (vertical orange rectangle) in the balancer haplotype, as observed in two independent Capture-C experiments. **b**, From top to bottom, wild-type and balancer Hi-C contact maps; $\log_2$[fold change] before normalization (balancer/wild type; red/blue); gene models; and differential gene expression (balancer/wild type). DE genes are shown in orange, non-DE genes in blue and non-tested genes (lowly expressed or lacking SNVs) in gray. Dotted vertical lines indicate TAD boundaries. **c**, Model of the inversion and associated changes in TAD structure and the position of three DE genes in the balancer haplotype.

at reduced frequencies for *sns*) despite changes in the genes' genomic context and relative distance, while in the other four cases, the loop is either lost or severely diminished in balancer chromosomes. For example, a long-range loop forms between the *sns* and *hbs* loci, separated by 6.25 Mb on the wild-type chromosome (Fig. 5a–d). On the balancer, these genes are separated by over 36.68 Mb (~20% of the size of the total *Drosophila* genome) spanning a centromere, and yet remarkably the looping interaction is still present (although at roughly half the interaction frequency), and there is no significant impact on the surrounding genes' expression.

In two other cases, the long-range loops normally span ~2 Mb (*CG4341/CG43403* and *eIF4E-4/PGRP-LA*), but are now separated by over 28 Mb in the balancer, which results in a severe reduction in looping frequency (Fig. 5e–h). Interestingly, this decrease does not affect the interacting genes' expression (for example, *CG4341/CG43403*; Fig. 5e–h). Two genes located further away from the looping region (*Elba2* and *CG31690*) have elevated expression on one side, while no genes change expression on the other. Similarly, the long-range loops between *Nufip/kug* (normally separated by 1.25 Mb) and *Wbp2/kug* (7.15 Mb) are separated by distances of 14.83 and 20 Mb, respectively, in the balancer (Supplementary Fig. 6). In both cases, this leads to a severe diminishment of the looping interactions, but this only seems to impact the expression of *CG10960*—a gene located close to *Wbp2* (Supplementary Fig. 6c,d). There is no significant difference in the expression of *Wbp2*, *Nufip* or *kug* (or other genes), despite the strong reduction in the associated looping interaction.

These inversions have enabled us to disentangle long-range looping interactions from gene expression. In some cases, the loop has a remarkable ability to form despite huge changes in genomic distance, suggesting that the underlying mechanism that brings these loci together can still function. In other cases, the inversion has broken (or severely diminished) the frequency of long-range interactions, and interestingly this has no effect on the interacting genes' expression. This indicates that long-range loop formation can be uncoupled from the associated genes' expression, suggesting no direct causal link between the two.

Discussion

Individual examples of genomic rearrangements that alter TAD structure[46] indicate that this can lead to mis-expression at specific loci[10,11,16–18,20]. These studies typically started with a phenotype (a structural variant leading to a developmental defect or cancer cells that have gained a selective advantage) and worked backwards to explain the mis-expression in the context of TAD structure. The balancer system may also have some selection bias as the original inversions were viable, before a lethal mutation and more X-ray-induced inversions were added. As they are homozygous lethal, balancers are always maintained in *trans*, and can therefore accommodate extensive recessive lethal rearrangements with loss or gain of regulatory interactions. This system thereby allowed us to ask more generally whether changes in chromatin topology can predict changes in gene expression, within the context of embryonic development.

A 38-kb inversion that overlaps a TAD boundary provides a good example (Fig. 6). Of the seven genes with allelic coverage within the affected TADs, only three are differentially expressed: *HGTX (Nkx6)*, *shd* and *dlp* (all essential embryonic genes). The *dlp* gene is directly disrupted by the inversion, while *HGTX* is impacted by the insertion of a transposable element. The only gene whose differential expression (overexpression in the balancer) is likely caused by a change in regulatory landscape is *shd*. The *shd* promoter normally establishes three-dimensional contacts across the left inversion breakpoint within TAD-A, as observed by Capture-C (Fig. 6a). These contacts are lost in the balancer, and new ones are formed with regions overlapping a DHS[43] originally located in TAD-B (orange highlight, Fig. 6a), suggesting that new enhancer–promoter interactions lead to *shd* mis-expression. However, such enhancer adoption did not occur for the other genes within the two rearranged TADs. This is not unique to this breakpoint; in all 16 inversion breakpoints that disrupt TADs, only a fraction of genes change expression, and generally not the closest genes (Supplementary Fig. 4d). This indicates that the activity of many regulatory elements is resistant to topological changes in their regulatory environment.

Our results, obtained from genetic rearrangements in *cis*, complement recent findings depleting CTCF[26,27] and cohesin[28–30] proteins in *trans*, where the majority of TADs were reduced, yet hundreds rather than thousands of genes changed expression[26,28,29]. This raises a number of interesting questions: what is the role of TADs in gene regulation? What are the regulatory differences between genes that are sensitive to, or resistant to, changes in their topology? Taken together, our results highlight an apparent uncoupling between gene expression and three-dimensional genome organization, and suggest that there must be properties, other than genome topology, that facilitate productive enhancer–promoter interactions.

Online content

Any methods, additional references, Nature Research reporting summaries, source data, statements of code and data availability and associated accession codes are available at https://doi.org/10.1038/s41588-019-0462-3.

Received: 5 December 2018; Accepted: 5 June 2019;
Published online: 15 July 2019

References

1. Bulger, M. & Groudine, M. Functional and mechanistic diversity of distal transcription enhancers. *Cell* **144**, 327–339 (2011).
2. Levine, M. Transcriptional enhancers in animal development and evolution. *Curr. Biol.* **20**, R754–R763 (2010).
3. Spitz, F. & Furlong, E. E. M. Transcription factors: from enhancer binding to developmental control. *Nat. Rev. Genet.* **13**, 613–626 (2012).
4. Furlong, E. E. M. & Levine, M. Developmental enhancers and chromosome topology. *Science* **361**, 1341–1345 (2018).
5. Jin, F. et al. A high-resolution map of the three-dimensional chromatin interactome in human cells. *Nature* **503**, 290–294 (2013).
6. Dixon, J. R. et al. Topological domains in mammalian genomes identified by analysis of chromatin interactions. *Nature* **485**, 376–380 (2012).
7. Nora, E. P. et al. Spatial partitioning of the regulatory landscape of the X-inactivation centre. *Nature* **485**, 381–385 (2012).
8. Rao, S. S. P. et al. A 3D map of the human genome at kilobase resolution reveals principles of chromatin looping. *Cell* **159**, 1665–1680 (2014).
9. Sexton, T. et al. Three-dimensional folding and functional organization principles of the *Drosophila* genome. *Cell* **148**, 458–472 (2012).
10. Lupiáñez, D. G. et al. Disruptions of topological chromatin domains cause pathogenic rewiring of gene-enhancer interactions. *Cell* **161**, 1012–1025 (2015).
11. Franke, M. et al. Formation of new chromatin domains determines pathogenicity of genomic duplications. *Nature* **538**, 265–269 (2016).
12. Tsujimura, T. et al. A discrete transition zone organizes the topological and regulatory autonomy of the adjacent *Tfap2c* and *Bmp7* genes. *PLoS Genet.* **11**, e1004897 (2015).
13. Narendra, V. et al. CTCF establishes discrete functional chromatin domains at the *Hox* clusters during differentiation. *Science* **347**, 1017–1021 (2015).
14. Guo, Y. et al. CRISPR inversion of CTCF sites alters genome topology and enhancer/promoter function. *Cell* **162**, 900–910 (2015).
15. Lettice, L. A. et al. Enhancer-adoption as a mechanism of human developmental disease. *Hum. Mutat.* **32**, 1492–1499 (2011).
16. Northcott, P. A. et al. Enhancer hijacking activates GFI1 family oncogenes in medulloblastoma. *Nature* **511**, 428–434 (2014).
17. Flavahan, W. A. et al. Insulator dysfunction and oncogene activation in *IDH* mutant gliomas. *Nature* **529**, 110–114 (2016).
18. Hnisz, D. et al. Activation of proto-oncogenes by disruption of chromosome neighborhoods. *Science* **351**, 1454–1458 (2016).
19. Northcott, P. A. et al. The whole-genome landscape of medulloblastoma subtypes. *Nature* **547**, 311–317 (2017).
20. Weischenfeldt, J. et al. Pan-cancer analysis of somatic copy-number alterations implicates *IRS4* and *IGF2* in enhancer hijacking. *Nat. Genet.* **49**, 65–74 (2017).

21. Shen, Y. et al. Deep functional analysis of synII, a 770-kilobase synthetic yeast chromosome. *Science* **355**, eaaf4791 (2017).
22. Shao, Y. et al. Creating a functional single-chromosome yeast. *Nature* **560**, 331–335 (2018).
23. Lee, H. et al. Effects of gene dose, chromatin, and network topology on expression in *Drosophila melanogaster*. *PLoS Genet.* **12**, e1006295 (2016).
24. Meadows, L. A., Chan, Y. S., Roote, J. & Russell, S. Neighbourhood continuity is not required for correct testis gene expression in *Drosophila*. *PLoS Biol.* **8**, e1000552 (2010).
25. Rodríguez-Carballo, E. et al. The HoxD cluster is a dynamic and resilient TAD boundary controlling the segregation of antagonistic regulatory landscapes. *Genes Dev.* **31**, 2264–2281 (2017).
26. Nora, E. P. et al. Targeted degradation of CTCF decouples local insulation of chromosome domains from genomic compartmentalization. *Cell* **169**, 930–944.e22 (2017).
27. Splinter, E. et al. CTCF mediates long-range chromatin looping and local histone modification in the β-globin locus. *Genes Dev.* **20**, 2349–2354 (2006).
28. Rao, S. S. P. et al. Cohesin loss eliminates all loop domains. *Cell* **171**, 305–320.e24 (2017).
29. Schwarzer, W. et al. Two independent modes of chromatin organization revealed by cohesin removal. *Nature* **551**, 51–56 (2017).
30. Wutz, G. et al. Topologically associating domains and chromatin loops depend on cohesin and are regulated by CTCF, WAPL, and PDS5 proteins. *EMBO J.* **36**, 3573–3599 (2017).
31. Oster, I. I. A new crossing-over suppressor in chromosome 2 effective in the presence of heterologous inversions. *Drosophila Inform. Serv.* **30**, 145 (1956).
32. Tinderholt, V. New mutants report. *Drosophila Inform. Serv.* **34**, 53–54 (1960).
33. Ashburner, M., Golic, K. G. & Hawley, R. S. *Drosophila: A Laboratory Handbook* (Cold Spring Harbor Laboratory Press, 2005).
34. Korbel, J. O. et al. Paired-end mapping reveals extensive structural variation in the human genome. *Science* **318**, 420–426 (2007).
35. Weischenfeldt, J., Symmons, O., Spitz, F. & Korbel, J. O. Phenotypic impact of genomic structural variation: insights from and for human disease. *Nat. Rev. Genet.* **14**, 125–138 (2013).
36. Mackay, T. F. C. et al. The *Drosophila melanogaster* genetic reference panel. *Nature* **482**, 173–178 (2012).
37. Zichner, T. et al. Impact of genomic structural variation in *Drosophila melanogaster* based on population-scale sequencing. *Genome Res.* **23**, 568–579 (2013).
38. Lindsley, D. L. & Zimm, G. G. *The Genome of Drosophila Melanogaster* (Academic Press, 1992).
39. Sudmant, P. H. et al. An integrated map of structural variation in 2,504 human genomes. *Nature* **526**, 75–81 (2015).
40. Miller, D. E. et al. The molecular and genetic characterization of second chromosome balancers in *Drosophila melanogaster*. *G3 (Bethesda)* **8**, 1161–1171 (2018).
41. Miller, D. E., Cook, K. R., Arvanitakis, A. V. & Hawley, R. S. Third chromosome balancer inversions disrupt protein-coding genes and influence distal recombination events in *Drosophila melanogaster*. *G3 (Bethesda)* **6**, 1959–1967 (2016).
42. Huang, W. et al. Natural variation in genome architecture among 205 *Drosophila melanogaster* genetic reference panel lines. *Genome Res.* **24**, 1193–1208 (2014).
43. Thomas, S. et al. Dynamic reprogramming of chromatin accessibility during *Drosophila* embryo development. *Genome Biol.* **12**, R43 (2011).
44. Ramírez, F. et al. High-resolution TADs reveal DNA sequences underlying genome organization in flies. *Nat. Commun.* **9**, 189 (2018).
45. Ogiyama, Y., Schuettengruber, B., Papadopoulos, G. L., Chang, J.-M. & Cavalli, G. Polycomb-dependent chromatin looping contributes to gene silencing during *Drosophila* development. *Mol. Cell* **71**, 73–88.e5 (2018).
46. Spielmann, M., Lupiáñez, D. G. & Mundlos, S. Structural variation in the 3D genome. *Nat. Rev. Genet.* **19**, 453–467 (2018).

Acknowledgements

We thank all members of the Furlong Laboratory for discussions and comments on the manuscript. We thank M. Davis, H. Gustafson, D. Garfield, T. Rausch and S. Waszak for useful discussions and suggestions at the various stages of the project. This work was technically supported by the EMBL Genomics Core Facility, with specific thanks to R. Hercog for WGS library preparation. This work was financially supported by an FRM grant (AJE20161236686) to Y.G.-H., the EMBL International PhD Programme to S.M., an EU Horizon 2020 Marie Skłodowska-Curie grant (708111) to A.J., an ERC starting grant (336045) to J.O.K. and ERC advanced grant DeCRyPT (787611) to E.E.M.F.

Author contributions

Y.G.-H. and E.E.M.F. designed the study. Y.G.-H., A.J., S.M., J.O.K. and E.E.M.F. analyzed the results. Y.G.-H., A.J., S.M. and E.E.M.F. wrote the manuscript. Y.G.-H. performed all of the experiments, except the mate-pair library experiment, which was performed by R.R.V. S.M. performed the SNV and structural variant calling and RNA-Seq analysis. A.J. performed the Hi-C and Capture-C data analysis. All authors discussed the results and commented on the manuscript.

Competing interests

The authors declare no competing interests.

Additional information

Supplementary information is available for this paper at https://doi.org/10.1038/s41588-019-0462-3.

Reprints and permissions information is available at www.nature.com/reprints.

Correspondence and requests for materials should be addressed to Y.G.-H., J.O.K. or E.E.M.F.

Publisher's note: Springer Nature remains neutral with regard to jurisdictional claims in published maps and institutional affiliations.

Methods

***Drosophila* lines.** To obtain the large number of embryos required for high-resolution Hi-C and Capture-C at specific embryonic stages, we set up a big cross between the two haplotypes. To obtain a large number of virgin wild-type female flies, we used a 'virginizer' line, w[1118]/(P{hs-hid}Y). We first made this line isogenic by backcrossing the w[1118]/(P{hs-hid}Y) line for at least 18 generations in single-pair matings to ensure maximum homozygosity. The resulting isogenic virginizer line was amplified to large amounts. To obtain females, vials containing embryos and larvae were placed in a 38 °C water bath for 1 h. This resulted in heat shock-induced expression of the pro-apoptotic gene *hid* on the Y chromosome, leading to the death of all males. The only adults that eclosed from these vials were female and therefore virgins. We refer to the virginizer line as the 'wild type' (+/+;+/+).

Adults from the wild-type isogenic line were crossed to the 'double-balancer' fly line (w; If/CyO; Sb/TM3,Ser) as follows (Supplementary Fig. 1a).

Cross 1. Male F_0 (If/CyO; Sb/TM3) × female F_0 (+/+;+/+). The F_1 offspring were composed of four genotypes in equal proportions: (If/+; Sb/+); (If/+;+/TM3); (+/CyO;+/TM3); and (+/CyO; Sb/+).

Cross 2 (backcross). Male F_1 (+/CyO;+/TM3) × female F_0 (+/+;+/+). The N_1 offspring (N_1^{pat}) were composed of four genotypes in equal proportions: (+/+;+/+); (+/+;+/TM3); (+/CyO;+/+); and (+/CyO;+/ TM3).

We also generated the reciprocal cross (yielding N_1^{mat} offspring) with female F_1 (+/CyO;+/TM3) × male F_0 (+/+;+/+).

The F_0 (+/+;+/+) and F_1 (+/CyO;+/TM3) adults were used for whole-genome and mate-pair sequencing. The pool of N_1 embryos was used for the RNA-Seq (N_1^{pat} and N_1^{mat}), Hi-C (N_1^{pat}) and Capture-C (N_1^{pat}) experiments. Additional controls were included for the RNA-Seq experiments (see below and Supplementary Fig. 1b).

Embryo collections. Freshly hatched adults were placed in embryo collection vials with standard apple cap plates. After three 1 h pre-lays, the flies were allowed to lay for 2 h, after which the embryos were aged to the appropriate time point. The embryos were then dechorionated using 50% bleach, and washed alternately with water and phosphate buffered saline (PBS) containing 0.1% Triton X-100. The embryos used for RNA-Seq were directly snap-frozen in liquid nitrogen. The embryos used for the Hi-C and Capture-C experiments were covalently crosslinked in 1.8% formaldehyde for 15 min at room temperature and stored at −80 °C.

Whole-genome and mate-pair sequencing. Genomic DNA from F_0 flies (+/+;+/+) and F_1 double-balancer flies (+/CyO;+/TM3) was isolated by grinding the flies in liquid nitrogen, followed by a 30-min incubation at 65 °C in lysis buffer (100 mM Tris-HCl (pH 7.5), 100 mM EDTA, 100 mM NaCl and 1% SDS). The sample was then treated with RNase A to degrade the RNA, before routine DNA extraction by phenol-chloroform and precipitation with ethanol.

The genomic DNA from these F_0 and F_1 samples was used to generate WGS libraries with an insert size of about 700 bp. The samples were sequenced on an Illumina MiSeq (300-bp paired end), yielding a total of 146 million and 68 million read pairs, respectively, corresponding to coverages of ~200× and ~100×.

The same F_0 and F_1 samples were used to generate mate-pair DNA libraries using the Nextera Mate Pair Sample Preparation Kit (Illumina) as previously described[47]. The samples were multiplexed and sequenced on an Illumina HiSeq 2000 (100-bp paired end). Nextera adapter contaminations were cleaned afterwards using NextClip version 1.3.1, yielding a total of 44 million and 73 million read pairs, respectively.

SNV and small indel calling. Both WGS and mate-pair sequencing data were mapped to dm6 using BWA-MEM[48] version 0.7.15. SNV and short indel calling was performed using FreeBayes[49] version 0.9.21–19 on the WGS data of both samples simultaneously and with disabled population priors. The results were filtered with vcflib (https://github.com/vcflib/vcflib) based on: a quality value of 30 or higher; a minimum of at least two reads carrying the allele to the right and to the left end; and the fact that the allele was seen on at least two reads mapping in each direction. The command used was: vcffilter -f 'QUAL > 29 & QUAL / AO > 2 & SAF > 1 & SAR > 1 & RPR > 1 & RPL > 1' -s. We further normalized indel variants, removed multi-allelic variants and decomposed multinucleotide substitutions (which are reported as haplotype blocks by FreeBayes) into SNVs using vt normalize[50]. Finally, we removed contigs other than chromosomes 2, 3 and X, obtaining a total of 860,095 SNVs in addition to 158,564 small indels.

Deletion calling. We applied Delly[51] version 0.7.2 on the WGS data of the F_0 and F_1 samples simultaneously and applied an extensive filtering procedure to reduce the number of false positive calls. From the initial 10,421 deletion calls, 5,150 dropped out that: were not flagged as QC PASS; were not on the main chromosomes (2, 3 or X); had a mapping quality value of less than 60; or did not match one of the expected genotypes (that is, balancer specific, wild-type specific and common, which together constituted >90% of the calls). Furthermore, we required a minimum number of supporting read pairs for reference and alternative alleles combined; namely, 40 read pairs for imprecise Delly calls or 25 split reads for precise Delly calls. Next, we developed a dynamic read-depth ratio filter that was applied to only large heterozygous calls (that is, balancer- or wild-type-specific ones). To this end, the read count within the predicted deletion was normalized by the summed read count in size-matched intervals flanking the locus (two flanking intervals; half the deletion size each), and these values were compared (absolute difference) between the two samples. We required a minimum difference in this read-depth ratio between samples with different allele counts, where this threshold adapts with structural variant size in a way that large structural variants need to show a clearer difference in the read-depth ratio between samples than small structural variants. Specifically, we set the threshold for the absolute difference between the balancer ratio and wild-type ratio to $1.25/(\text{deletion base pairs})^{0.2} + 0.5$. To give an example, this filter removed a number of obviously false calls above 100 kb. Deletions were overlapped with a mappability map to classify them into high- (at least 50% of the structural variant is in a uniquely mappable region) or low-confidence loci. This resulted in four call sets: 3,072 high-confidence calls <50 bp; 737 high-confidence calls in the range between 50 and 159 bp; 395 high-confidence large calls (≥160 bp); and 75 low-confidence large calls (≥160 bp).

Finally, we merged Delly deletion calls with small deletions called by FreeBayes (which underlie the aforementioned filtering criteria) and chose a lower size cutoff of 15 bp. During the merging process, FreeBayes calls were given priority over matching Delly calls (based on the 50% reciprocal overlap criterion). The final dataset (referred to as 'deletions' in the main text) contains 8,340 deletions on chromosomes 2, 3 and X; namely: 7,114 deletions below 50 bp; 756 deletions in the 50–159-bp range; and 470 large deletions (≥160 bp). Of these, 6,180, 687 and 434, respectively, were located on chromosomes 2 and 3. Taking only the allele-specific ones, 4,919 deletions below 50 bp, 549 deletions in the 50–159-bp range and 434 large deletions (≥160 bp) remained.

We compared these balancer deletion calls to deletions present in the DGRP lines (inbred lines generated from wild isolates). We found that the deletions present in the DGRP line tended to be smaller on average compared with the balancer chromosomes. Besides, 50% of the small (20–50-bp) wild-type-specific deletions were found in the DGRP lines versus 40% for the balancer-specific ones. This is in line with our overall findings that the double-balancer chromosomes accumulate mutations not naturally present in the wild.

PCR validation of deletion calls. To validate deletion calls, we performed PCR on randomly selected loci in three categories: 25 loci of 50–159 bp in size; 25 loci above 159 bp with high confidence; and 25 loci above 159 bp with low confidence. We designed primers using a lab-internal extension to Primer3 (ref. [52]). The PCR reactions (under standard conditions) were performed on genomic DNA extracted from F_1 (+/CyO;+/TM3) and F_0 (+/+;+/+) adult flies to visualize a shift in the size of the PCR product. In the size range 50–159 bp, 24 out of 25 loci validated; 24/25 loci validated for high-confidence calls of ≥160 bp; and 25/25 loci validated for low-confidence calls. This yielded an estimated FDR of 2.66%. After weighting by the number of deletion calls in each of these categories, we can estimate an FDR of 3.75%.

Duplication calling and filtering. Delly[51] version 0.7.5 was run in tandem duplication mode and supplied with both mate-pair and WGS libraries for F_0 and F_1 samples simultaneously. Duplication calls were initially filtered by the quality PASS criteria and by their combined genotypes, which were required to be heterozygous in the F_1 sample. We did not require homozygosity in the F_0 sample because many homozygous tandem duplications are wrongly classified as heterozygous (this misclassification is a known issue of the classifier function, according to the author of Delly), and due to the fact that reference sequence overlapping the breakpoint of homozygous tandem duplication remains contiguous. For all remaining 352 calls, we generated quality control plots that contained a total read-depth track, a mappability track and, importantly, a B-allele frequency measured at SNV positions around the predicted locus. These plots allowed us to sort out false positives, leaving 122 manually curated high-quality tandem duplications.

Aside from tandem duplications, we inspected the B-allele frequency ratio across the genomes and unraveled three non-tandem duplications of 4.3, 10.4 and 258 kb in size. The final set (referred to as 'duplications' in the main text) contained 125 duplications.

Refinement of inversion breakpoints on the balancer chromosomes. Approximate breakpoint locations were estimated from an initial inspection of the balancer-specific Hi-C plots and narrowed down to ~10 kb. To identify the exact breakpoints, we ran Delly[51] version 0.7.1 in inversion and translocation mode (because chromosomes are split into p- and q-arms, some intra-chromosomal rearrangements will be reported as translocation calls) on both samples, using both mate-pair and WGS libraries separately. As translocation calls are typically very noisy, we only searched the regions of interest for calls that connect the expected loci. Starting from Hi-C-based coordinates, we scanned a region of 200 kb around each breakpoint and identified 14 out of 16 rearrangement junctions in the mate-pair data, 12 of which were additionally in the paired-end data. A single inversion could not be found as one of its breakpoints is likely outside the known reference

genome. As exact breakpoints of these structural variants underlie an inevitable alignment uncertainty, we manually determined the exact base position of the breakpoints that best matches the read mapping. Interestingly, Miller et al.[40,41] unraveled the exact breakpoints of multiple balancer chromosomes including TM3 shortly after this analysis and our results match perfectly to their findings. Also, they were not able to resolve the last inversion, for which we provide a 'best guess' according to Integrative Genomics Viewer inspection and a search for dangling read pairs (that is, where only one of the reads maps). These results are summarized in Supplementary Table 2. At one breakpoint (20.32 Mb on chromosome 3R), we observed a 17.5-kb balancer-specific deletion that not was identified in the previous characterization of the balancer chromosome TM3 (ref. [41]). Note that we found no heterozygous SNVs in the putative deletion region.

We manually validated smaller (non-nested) Delly inversion calls against Hi-C contact maps, and took into further consideration one 38-kb inversion that was supported by our Hi-C data.

Fly crosses for RNA-Seq experiments. RNA-Seq was performed on *Drosophila* embryos of the N_1 generation at 6–8 h after egg laying (stages 10 and 11) (Supplementary Fig. 1; see Methods section on fly lines). The genotypes of the *Drosophila* embryos cannot be phenotypically distinguished at this early developmental stage; hence, the resulting libraries consist of a pool of four different genotypes where 25% of chromosomes 2 and 3 are balancer chromosomes (CyO and TM3, respectively) and 75% are wild type. As we anticipated a bias from maternally deposited messenger RNAs (mRNAs; that is, an excess of RNA from the female parental line), we implemented two critical steps to overcome this problem. First, we manually removed unfertilized eggs among the embryos before library preparation, which likely contribute to the biggest part of maternal mRNAs. Second, we collected fly embryos from parents where the N_1 backcross was set up in both directions: N_1^{pat} (using F_1 males and wild-type parental females) as well as N_1^{mat} (using F_1 females and wild-type parental males). The impact of maternal mRNAs for any given gene will act in opposite directions in both samples, allowing us to control for such effects.

To determine the impact of *trans* effect, we used adult fly heads from single-balancer lines (used in Supplementary Fig. 3a). These lines are based on the same F_0 wild-type line as the double-balancer line and denoted F_1^{CyO} and F_1^{TM3} (for chromosome 2 balanced and chromosome 3 balanced, respectively). In parallel, adult fly heads from the double-balancer F_1 line were collected (denoted $F1^{CyO;TM3}$; used in Supplementary Fig. 3b). In addition, we collected female-only fly heads from the F_1 cross (denoted F_1^{female}) to assess the biological noise between two lines that both carry the CyO and TM3 balancer chromosomes but have originated from a different cross (comparing F_1^{female} and $F_1^{CyO;TM3}$).

RNA-Seq experiments. For RNA isolation, a pool of approximately 100 embryos or 20 adult fly heads was homogenized in TRIzol LS (Life Technologies) with a Cordless Motor for Pellet Mix and pestels (VWR) on ice. RNA was extracted according to the manufacturer's instructions, and the remaining DNA was digested with RNase-free DNase I (Roche) for 30 min. The RNA solution was purified a second time using Agencourt RNAClean XP beads (Beckman Coulter).

Strand-specific RNA-Seq was performed from 1 µg of total RNA using the NEBNext Ultra Directional RNA Library Prep Kit for Illumina (NEB) according to the manufacturers' recommendations. RNA-Seq was performed on embryos from the N_1^{pat} and N_1^{mat} lines, each in two biological replicates. The samples were multiplexed and sequenced on an Illumina NextSeq 500 (150-bp paired end).

We also generated RNA-Seq libraries for the controls mentioned above: four adult fly lines (F_1^{CyO}, F_1^{TM3}, $F_1^{CyO;TM3}$ and F_1^{female}; each in two biological replicates) sequenced on the Illumina HiSeq 2000 (100-bp paired end) or NextSeq (150-bp paired end). An overview of the sequencing depth is provided in Supplementary Table 4.

Differential RNA-Seq analysis. The RNA-Seq data were mapped to the *D. melanogaster* reference genome dm6, and the reads separated into the haplotypes based on overlap with haplotype-tagging SNVs. A custom script based on pysam (https://github.com/pysam-developers/pysam) detects such overlaps and integrates information across all SNVs within a read pair. This way, read pairs with conflicting information (that is, containing both balancer- and wild-type-tagging SNVs) can be filtered; this fraction was below 0.2% of read pairs in all cases. In the embryonic RNA-Seq dataset (2× 144-bp reads after demultiplexing), ~28% of read pairs could be assigned to haplotypes (see Supplementary Table 4). We then counted fragments per haplotype per gene using HTSeq-counts[53].

We tested genes for differential expression by inserting these haplotype-specific counts for all four replicates (2× N_1^{pat} and 2× N_1^{mat}) into a matrix and supplying it to DESeq2 (ref. [54]). Our experimental design (that is, examining RNA-Seq from embryos obtained from the reciprocal crosses) takes care of any potential influences of maternally deposited mRNAs. DESeq2 could thereby test for differential expression against a 25% ratio with the multiple replicates (from the reciprocal crosses). Genes were filtered for a minimum number of reads (an average of 50 fragments from both haplotypes per gene per sample) and by chromosome (only chromosomes 2 and 3 were considered). The resulting *P* values were corrected using fdrtool[55], identifying 512 differentially expressed genes (two-sided Wald test; 5% FDR) and 4,845 non-differentially expressed genes. The remaining 9,053 genes were not tested for differential expression due to a low number of reads, but were further divided into 4,989 lowly expressed separable genes (for which at least one RNA-Seq read could be haplotype separated) and 4,064 inseparable genes. If the former, lowly expressed genes did change in their expression (that is, were activated in the balancer) due to rearrangements, we would be able to detect them.

To assess whether the 512 differentially expressed genes are enriched in Gene Ontology terms, we compared them to all 5,357 testable expressed genes using the PANTHER over-representation test (http://pantherdb.org/tools/compareToRefList.jsp). We found no significant enrichment (Bonferroni-corrected P value < 0.05, Fisher's exact test) for any of the annotation datasets used (PANTHER GO-Slim Molecular Function, Biological Process or Cellular Component), indicating that the differentially expressed genes have heterogenous functions.

Controlling for *trans* effects in the RNA-Seq data. To control for potential *trans* effects (Supplementary Fig. 3a,b), we generated three F_1 generations of adult flies with different genotypes: one line with only chromosome 2 balanced (CyO); one with only chromosome 3 balanced (TM3); and one carrying both balancer chromosomes (double balancer, or normal F_1 cross; see also Methods section 'Fly crosses for RNA-Seq experiments'). Note that in this design, allele separation is only feasible on the balanced chromosomes themselves. Apart from two haplotypes (balancer or wild type), we also considered two balancer genotypes (single or double balancer). We then tested the interaction term between haplotype and balancer genotype on gene expression, using the DESeq2 formula ~ Haplotype + Balancer.Genotype + Haplotype:Balancer.Genotype. For example, in the case of CyO, we asked whether the differential expression (balancer versus wild type) of a gene is significantly different when using the CyO cross (which does not contain TM3) compared with using the double-balancer cross (which contains TM3). Biological noise was estimated by comparing the new F_1 double-balancer cross ($F_1^{CyO;TM3}$) with a (female) F_1^{female} line with the same interaction approach, asking whether old versus new sequencing data significantly changes differentially expressed genes. Here, due to lower sequencing depth, we reduced the threshold for a minimum number of reads to 30 fragments.

Assessing the overlap of CNVs with genes. We required at least one exon of a gene to overlap a CNV (deletion or duplication). Additionally (with the exception of Fig. 2b and Supplementary Fig. 3c), for deletions in the wild type and duplications in the balancer, we required the gene to show increased expression in the balancer compared with the wild type. Conversely, for deletions in the balancer and duplications in the wild type, we required the gene to show a decreased expression in the balancer.

Capture-C primer design. As Capture-C viewpoints, we used DpnII restriction fragments, which satisfy the following criteria in the context of SNVs and small indels: (1) length ≥ 124 bp; (2) restriction sites (recognition sequences) at both ends are not disrupted in either of the haplotypes; and (3) no restriction sites are created inside the fragment in either of the haplotypes.

We also imposed additional criteria on the two candidate 120-bp probes starting from the restriction sites and continuing into the restriction fragment. The following criteria had to be satisfied by both of the probes: (1) GC content in the range of 0.25–0.65 (≤20 repeat-masked base pairs); (2) no secondary BLAT alignment score of ≥10; (3) no more than 1 bp of allele-specific SNVs; and (4) no allele-specific small indels.

We incorporated the shared SNVs and shared small indels into the probe sequences. We also resolved the possible allele-specific SNVs in a way that the probe has an allele different from the wild-type and different from the balancer, and no new restriction sites are created. All of the viewpoints and probe sequences are given in Supplementary Table 6.

In total, we designed 314 Capture-C viewpoints manually assigned to 328 genes; namely: 226 differentially expressed genes; 69 non-differentially expressed genes; and 33 non-tested genes. Some of the viewpoints were assigned to more than one gene (Supplementary Table 6). Seven of the viewpoints overlapped allele-specific SNVs and were therefore excluded from any analysis. The remaining 307 Capture-C viewpoints are assigned to 321 genes; namely: 221 differentially expressed genes; 68 non-differentially expressed genes; and 32 non-tested genes.

Hi-C and Capture-C library preparation. *Drosophila* embryos were collected at 4–8 h after egg laying (stages 8–11) from the N_1^{pat} generation, consisting of a backcross between male F_1 double-balancer flies (that is, +/CyO;+/TM3) and female F_0 flies (that is, +/+;+/+). Embryos were fixed and nuclei were extracted as described previously[56]. For Hi-C, three aliquots of 30×10^6 nuclei in two biological replicates were used for each 3C template preparation. The Hi-C libraries were prepared as previously described[9], using DpnII as a restriction enzyme. The final library was prepared, using the NEBNext Ultra DNA Library Prep Kit for Illumina according to the manufacturer's instructions, from at least 1 µg of DNA. The libraries were sequenced on the Illumina HiSeq 2000 (100-bp paired end).

The Capture-C libraries were prepared as previously described[57], using DpnII as a restriction enzyme and performing the ligation step 'in nucleus'. The template

was then processed with the Roche Nimblegen SeqCap EZ Library SR system and a double-capture strategy. The libraries were sequenced on the Illumina NextSeq (150-bp paired end).

Hi-C and Capture-C data processing. Hi-C sequencing reads were mapped onto the *D. melanogaster* reference genome dm6, considering both reads from a read pair separately, using BWA-MEM[48] with options -E50 -L0 -5. After merging the paired reads, we annotated them with haplotypes based on SNVs. Using pairsamtools (https://github.com/mirnylab/pairsamtools), we formed Hi-C pairs in pairsam format, selected only linear–linear or rescued chimeric–linear pair types, and sorted and de-duplicated them. Reads were then separated according to their haplotype, removing supplementary alignments, splitting read pairs into separate BAM files, and filtering and processing them using HiCExplorer[44], using hicBuildMatrix with options --restrictionSequence GATC --danglingSequence GATC --binSize 5000 --skipDuplicationCheck. The resulting contact matrices were summed across two biological replicates and normalized by iterative correction using hicCorrectMatrix with options --filterThreshold -1.5 5, taking only chromosomes 2, 3, 4, X and Y.

To obtain balancer contact maps in the balancer genome assembly, we relied on the separate BAM files obtained by splitting read pairs. We used CrossMap[58] with a custom chain file to convert them from the reference assembly to the balancer assembly. We then processed them using HiCExplorer as described above.

Capture-C sequencing reads were processed in the same manner, up to and including filtering them using HiCExplorer. We further processed the filtered reads using CHiCAGO[59] to obtain contact count tracks in restriction fragment resolution for each replicate, haplotype and viewpoint.

TAD calling. To call TADs from Hi-C data, we used an approach based on the TAD separation score, using hicFindTADs from HiCExplorer with default options. We calculated TAD separation score profiles for seven different window sizes, ranging from 50–195 kb. The TAD separation score is calculated as the average *Z*-score of all Hi-C contacts between an adjacent window upstream and an adjacent window downstream. We then averaged these profiles into an aggregate insulation score profile. To ensure that the profile incorporates the proper genomic context around rearrangement junctions, we used the balancer genome assembly to calculate the insulation score profile for balancer chromosomes and the reference assembly for wild-type chromosomes. We then converted the balancer profile to the reference assembly.

To compare the insulation score profiles between replicates and haplotypes (Supplementary Fig. 4a), we processed the Hi-C data from two biological replicates separately, and for each replicate downsampled the wild-type haplotype reads to match the number of reads of the balancer haplotype.

Differential TAD analysis. As described above, from the wild-type Hi-C contact map, we identified 767 wild-type TAD boundaries (separating 771 TADs) in chromosomes 2 and 3. In the same manner, we identified 757 balancer TAD boundaries (separating 761 TADs) in these two chromosomes from the balancer Hi-C contact map in the balancer genome assembly. We then converted the balancer TAD boundaries to the reference genome assembly to compare these two sets of boundaries. To account for the difficulty in accurately calling TAD boundaries, we compared them against boundaries called with a less stringent *P* value threshold (using hicFindTADs with option --thresholdComparisons 0.1) and allowed the boundaries to be shifted by up to 25 kb between haplotypes. This identified 671 matched TAD boundaries, 96 wild-type-specific ones and 86 balancer-specific ones.

In addition to allele-specific TAD boundaries, inversion breakpoints on the balancer chromosomes also shuffle TADs, causing them to be resized (Fig. 3h). Out of the 16 disrupted TADs, five also have an allele-specific boundary on one side: three balancer specific (change of boundary up to 136 kb) and two wild-type specific (change up to 65 kb). While analysing these TADs, we considered their wild-type boundaries and the set of 161 genes with TSSs located within these boundaries. In the balancer, 15 of the considered genes (two of which are differentially expressed genes) are across a balancer-specific boundary (outside the disrupted TAD), while eight genes (two of which are differentially expressed genes) located within the disrupted TADs were not considered due to being located across a wild-type-specific boundary in the wild-type haplotype.

Differential Hi-C contact analysis. Differential Hi-C analysis was performed on contact maps before normalization and before summing biological replicates. For each replicate and haplotype, we fitted a distance-decay trend using the R package locfit[60] and provided the fitted values as normalization factors in DESeq2 (ref. [54]). We compared the haplotypes for all 453,423 Hi-C contacts within 100 kb that were not separated by large nested inversions. Contacts with low average count numbers were excluded in the independent filtering procedure, leaving 216,066 Hi-C contacts to be tested. Out of those, 5,297 were differential (two-sided Wald test; 10% FDR). We excluded differential contacts that had at least 1 kb of overlap with CNVs at either of the interacting 5-kb bins, leaving 4,329 high-confidence differential Hi-C contacts. Of those, 4,299 had an absolute fold change of >1.5 (that is, a fold change >1.5 or <2/3, equivalent to an absolute $\log_2$[fold change] > $\log_2$[1.5]) between the two haplotypes.

Differential Capture-C contact analysis. The reference genome dm6 was digested in silico into restriction fragments using the sequence GATC recognized by the restriction enzyme DpnII. The restriction fragments were further filtered in the context of SNVs, small indels and structural variants, removing: (1) restriction fragments with a disrupted restriction site (a different sequence from the recognition sequence) at either end in either of the haplotypes; and (2) restriction fragments with an additional restriction site created in either of the haplotypes.

We considered jointly the Capture-C interactions originating from the 307 viewpoints that did not overlap structural variants. We compared the haplotypes for all 561,958 Capture-C contacts within 100 kb from the viewpoint that were not separated by large nested inversions. Contacts with low average count numbers were excluded in the independent filtering procedure, leaving 59,605 Capture-C contacts to be tested. Out of those, 984 were differential (two-sided Wald test; 5% FDR). We excluded differential contacts to restriction fragments whose restriction site overlaps a deletion or duplication (but allowed smaller deletions and duplications that were fully contained between the restriction sites). This resulted in 935 differential Capture-C contacts, of which we used 931 that had an absolute fold change of >1.5.

Correlating differential contacts and differential gene expression. We aligned and oriented the genes by their 5′-most TSS, and considered the differential Hi-C contacts between the TSS and the surrounding genomic region. When considering Capture-C data viewpoints associated with multiple genes, we took them into account multiple times, each time in association with a different gene. Averaging within differentially expressed genes and non-differentially expressed genes separately, the average number of differential contacts from the TSS to a given relative location was plotted.

Genomic features overlap. We used DHSs at the same stages of embryogenesis from ref. [43], merging the peaks from stages 9–11 and converting the resulting dataset to the reference genome dm6. Promoters were defined by taking all annotated TSSs from FlyBase release FB2015_02 and extending them by ±1 kb. Enhancers were combined from CAD[61] and mesoderm CRMs[62] converted to dm6. Distal enhancers were defined as DHSs overlapping an enhancer and not overlapping any promoters.

For the purpose of overlapping with other genomic features (Supplementary Fig. 5c), differential Hi-C contacts between two genomic bins were contributing twice, with each of the bins serving as either viewpoint or the other end. For the same purpose, differential Capture-C contacts were reduced into 445 clusters, by extending the interacting restriction fragments by ±1 kb and merging the overlapping ones for each viewpoint. Permutation tests were performed by keeping the viewpoints fixed and randomly shuffling the distances to the other ends of the interactions. The sign of these distances was also randomly flipped. The 95% confidence intervals and *P* value were derived from the overlaps obtained for 1,000 random shuffles.

Statistics. We performed differential gene expression, differential Hi-C and differential Capture-C analyses using the two-sided Wald test integrated in DESeq2 (ref. [54]). For differential gene expression, we corrected the resulting *P* values by re-estimating the variance of the null model using fdrtool[55]. All of the other statistical tests are discussed in the context of the analysis for which they were applied, in the corresponding Methods subsections above.

Reporting Summary. Further information on research design is available in the Nature Research Reporting Summary linked to this article.

Data availability

All raw data, which consist of 75 demultiplexed files, were submitted to ArrayExpress (https://www.ebi.ac.uk/arrayexpress/browse.html) under accession numbers E-MTAB-7510 (whole-genome and mate-pair sequencing), E-MTAB-7512 (Hi-C), E-MTAB-7513 (Capture-C) and E-MTAB-7511 (RNA-Seq). The Hi-C contact maps, RNA-Seq read counts and other processed data are available on the Furlong Laboratory web page at http://furlonglab.embl.de/data.

Code availability

Custom code used for the analysis is available at https://github.com/ajank/balancer-paper.

References

47. Mardin, B. R. et al. A cell-based model system links chromothripsis with hyperploidy. *Mol. Syst. Biol.* **11**, 828 (2015).
48. Li, H. Aligning sequence reads, clone sequences and assembly contigs with BWA-MEM. Preprint at https://arxiv.org/abs/1303.3997 (2013).
49. Garrison, E. & Marth, G. Haplotype-based variant detection from short-read sequencing. Preprint at https://arxiv.org/abs/1207.3907 (2012).
50. Tan, A., Abecasis, G. R. & Kang, H. M. Unified representation of genetic variants. *Bioinformatics* **31**, 2202–2204 (2015).

51. Rausch, T. et al. DELLY: structural variant discovery by integrated paired-end and split-read analysis. *Bioinformatics* **28**, i333–i339 (2012).
52. Untergasser, A. et al. Primer3—new capabilities and interfaces. *Nucleic Acids Res.* **40**, e115 (2012).
53. Anders, S., Pyl, P. T. & Huber, W. HTSeq—a Python framework to work with high-throughput sequencing data. *Bioinformatics* **31**, 166–169 (2015).
54. Love, M. I., Huber, W. & Anders, S. Moderated estimation of fold change and dispersion for RNA-Seq data with DESeq2. *Genome Biol.* **15**, 550 (2014).
55. Strimmer, K. fdrtool: a versatile R package for estimating local and tail area-based false discovery rates. *Bioinformatics* **24**, 1461–1462 (2008).
56. Bonn, S. et al. Tissue-specific analysis of chromatin state identifies temporal signatures of enhancer activity during embryonic development. *Nat. Genet.* **44**, 148–156 (2012).
57. Davies, J. O. J. et al. Multiplexed analysis of chromosome conformation at vastly improved sensitivity. *Nat. Methods* **13**, 74–80 (2016).
58. Zhao, H. et al. CrossMap: a versatile tool for coordinate conversion between genome assemblies. *Bioinformatics* **30**, 1006–1007 (2014).
59. Cairns, J. et al. CHiCAGO: robust detection of DNA looping interactions in Capture Hi-C data. *Genome Biol.* **17**, 127 (2016).
60. Loader, C. *locfit: Local Regression, Likelihood and Density Estimation* https://CRAN.R-project.org/package=locfit (2013).
61. Cusanovich, D. A. et al. The *cis*-regulatory dynamics of embryonic development at single-cell resolution. *Nature* **555**, 538–542 (2018).
62. Zinzen, R. P., Girardot, C., Gagneur, J., Braun, M. & Furlong, E. E. M. Combinatorial binding predicts spatio-temporal *cis*-regulatory activity. *Nature* **462**, 65–70 (2009).

nature research

Corresponding author(s): Furlong EE

Last updated by author(s): May 2, 2019

Reporting Summary

Nature Research wishes to improve the reproducibility of the work that we publish. This form provides structure for consistency and transparency in reporting. For further information on Nature Research policies, see Authors & Referees and the Editorial Policy Checklist.

Statistics

For all statistical analyses, confirm that the following items are present in the figure legend, table legend, main text, or Methods section.

n/a	Confirmed	
☐	☒	The exact sample size (*n*) for each experimental group/condition, given as a discrete number and unit of measurement
☐	☒	A statement on whether measurements were taken from distinct samples or whether the same sample was measured repeatedly
☐	☒	The statistical test(s) used AND whether they are one- or two-sided *Only common tests should be described solely by name; describe more complex techniques in the Methods section.*
☐	☒	A description of all covariates tested
☐	☒	A description of any assumptions or corrections, such as tests of normality and adjustment for multiple comparisons
☐	☒	A full description of the statistical parameters including central tendency (e.g. means) or other basic estimates (e.g. regression coefficient) AND variation (e.g. standard deviation) or associated estimates of uncertainty (e.g. confidence intervals)
☐	☒	For null hypothesis testing, the test statistic (e.g. *F*, *t*, *r*) with confidence intervals, effect sizes, degrees of freedom and *P* value noted *Give P values as exact values whenever suitable.*
☒	☐	For Bayesian analysis, information on the choice of priors and Markov chain Monte Carlo settings
☒	☐	For hierarchical and complex designs, identification of the appropriate level for tests and full reporting of outcomes
☐	☒	Estimates of effect sizes (e.g. Cohen's *d*, Pearson's *r*), indicating how they were calculated

Our web collection on statistics for biologists contains articles on many of the points above.

Software and code

Policy information about availability of computer code

Data collection	Illumina built-in software for MiSeq, HiSeq 2000 and NextSeq 550 sequencers
Data analysis	bwa mem 0.7.15 CHiCAGO 1.1.8 DELLY 0.7.1, 0.7.2 and 0.7.5 DESeq2 1.16.1 fdrtool 1.2.15 FreeBayes v0.9.21-19 ggbio 1.24.1 HiCExplorer 2.0 HTSeq 0.7.2 locfit 1.5-9.1 NextClip 1.3.1 pairsamtools 0.0.1-dev PANTHER 14.1 Primer3 2.3.5 pysam 0.9.0 R 3.4.0 samtools 1.7 Snakemake 4.8.1 vcflib v1.0.0-rc1 vt v0.5772-60f436c3

For manuscripts utilizing custom algorithms or software that are central to the research but not yet described in published literature, software must be made available to editors/reviewers. We strongly encourage code deposition in a community repository (e.g. GitHub). See the Nature Research guidelines for submitting code & software for further information.

Data

Policy information about availability of data

All manuscripts must include a data availability statement. This statement should provide the following information, where applicable:

- Accession codes, unique identifiers, or web links for publicly available datasets
- A list of figures that have associated raw data
- A description of any restrictions on data availability

All raw data, which consist of 75 demultiplexed files of whole-genome and mate-pair sequencing, Hi-C, Capture-C and RNA-seq were submitted to ArrayExpress (https://www.ebi.ac.uk/arrayexpress/browse.html) under accession numbers: E-MTAB-7510 (whole-genome and mate-pair sequencing), E-MTAB-7512 (Hi-C), E-MTAB-7513 (Capture-C) and E-MTAB-7511 (RNA-seq). The Hi-C contact maps, RNA-seq read counts and other processed data are available on the Furlong lab web page, http://furlonglab.embl.de/data.

Field-specific reporting

Please select the one below that is the best fit for your research. If you are not sure, read the appropriate sections before making your selection.

☒ Life sciences ☐ Behavioural & social sciences ☐ Ecological, evolutionary & environmental sciences

For a reference copy of the document with all sections, see nature.com/documents/nr-reporting-summary-flat.pdf

Life sciences study design

All studies must disclose on these points even when the disclosure is negative.

Sample size	Sample size (n=2) is indicated, and sufficient to compare double balancer and virginizer haplotypes, as implied by the crossing scheme. Two haplotypes were directly compared in cis.
Data exclusions	One Capture-C experiment, with two biological replicates (out of 289 experiments with replicates) had non-uniform allelic ratio, differing from the expected 1:3 ratio, and was therefore flagged as failed and excluded from the analysis. The exclusion criteria were not pre-established.
Replication	Two biological replicates were performed for all Hi-C, Capture-C and RNA-seq experiments. Moreover, we used single-balancer fly lines to verify the near absence of trans effects on gene expression (Supplementary Fig. 3a) and assessed the biological noise between two double-balancer lines originating from a different cross (Supplementary Fig. 3b). We also confirmed that Insulation Score profiles derived from Hi-C data are stable across replicates (Supplementary Fig. 4a). All these attempts at replication were successful.
Randomization	Not applicable: As this is an observational genetics study, randomized allocation into experimental groups is not relevant. To limit potentially confounding batch effects, we sequenced the libraries of different samples and replicates for the same experiment on the same flow cell where possible.
Blinding	The Core facility where the sequencing was performed had no access to the sample genotypes. Due to the asymmetric nature of the crossing scheme (Supplementary Fig. 1), blinding during the data analysis was not possible.

Reporting for specific materials, systems and methods

We require information from authors about some types of materials, experimental systems and methods used in many studies. Here, indicate whether each material, system or method listed is relevant to your study. If you are not sure if a list item applies to your research, read the appropriate section before selecting a response.

Materials & experimental systems

n/a	Involved in the study
☒	☐ Antibodies
☒	☐ Eukaryotic cell lines
☒	☐ Palaeontology
☐	☒ Animals and other organisms
☒	☐ Human research participants
☒	☐ Clinical data

Methods

n/a	Involved in the study
☒	☐ ChIP-seq
☒	☐ Flow cytometry
☒	☐ MRI-based neuroimaging

Animals and other organisms

Policy information about studies involving animals; ARRIVE guidelines recommended for reporting animal research

Laboratory animals	Species: Drosophila melanogaster Strain: Double balancer and virginizer Sex: Female or mixed sexes

	Age: embryos 4-8h or 6-8h after agg lay, or young adults
Wild animals	The study did not involve wild animals.
Field-collected samples	The study did not involve samples collected from the field.
Ethics oversight	No ethical approval or guidance was required. Drosophila melanogaster is an invertebrate, and as such is not considered as an animal.

Note that full information on the approval of the study protocol must also be provided in the manuscript.